New Accelerating Tube for 4 MV Van de Graaff Accelerator

AUTHOR(S):

FUKUZAWA, Fumio; OGINO, Koya; TOMITA, Michio; YOSHIDA, Koji; NORISAWA, Keizo; SAKISAKA, Masakatsu

CITATION:

FUKUZAWA, Fumio ...[et al]. New Accelerating Tube for 4 MV Van de Graaff Accelerator. Memoirs of the Faculty of Engineering, Kyoto University 1973, 35(1): 52-78

ISSUE DATE:

1973-01

URL:

http://hdl.handle.net/2433/280907

New Accelerating Tube for 4 MV Van de Graaff Accelerator

By

Fumio FUKUZAWA,* Koya OGINO,* Michio TOMITA,* Koji YOSHIDA,* Keizo NORISAWA* and MASAKATSU SAKISAKA*

(Received September 30, 1972)

The accelerating tube with diametrically magnetized ring magnets for the bending of backstreaming electrons was constructed for the 4 MV Van de Graaff accelerator of Kyoto University. The X-ray yield due to the electron loading was reduced to a factor of about 100 ; and the ion beam current was increased by a factor of about five compared with that of the old tube which had plane electrodes with small accelerating apertures. Characteristics of evacuation, beam convergence and accelerator operation are described ; and typical results of ion analysis are given for hydrogen, helium, nitrogen, neon and argon.

1. Introduction

Electron loading is the most important factor affecting the characteristics of a static accelerator. Methods of suppression of electron loading are classified into the following three types :

(1) Use of electrodes with very small accelerating apertures.

(2) Use of an inclined field accelerating tube.

(3) Application of a transverse magnetic field across the accelerating tube.

Types of (1) and (2) have been used in practice. Type (1) allows the use of plane electrodes and simplifies the structure of the accelerating tube. The structure of the inclined field tube of type (2) is rather complicated, but the suppression of electron loading is complete. On the other hand, the method (3) has only recently been successfully realized in the accelerators of Kyushu University[1] and of A. W. R. E.[2], with reports of its excellent features.

In our laboratory, the 4 MV Van de Graaff accelerator of type (1) had been used for a few years. Small conductance of the accelerating tube caused a rather poor vaccuum near the exit of the ion source. This is unfavorable especially for

* Department of Nuclear Engineering

heavy ion accelerations. In order to enlarge the conductance of the accelerating tube, the accelerating apertures must be widened. But the wide aperture causes a large amount of electron loading and the maximum terminal voltage is lowered. We have newly constructed the accelerating tube of type (3), whose electrodes are bucket type with large accelerating apertures.

The amount of the electron loading has conveniently been represented by the X-ray yields at various points of accelerating tube. Measurements of X-rays were made for the accelerator with bucket type electrodes by S. Takayanagi et al[3], and for the one with plane electrodes by E. Teranishi and M. Kageyama[4]. We have made such measurements for both the old and the new accelerating tubes, and compared their characteristics. With the same outer dimensions of the accelerating tubes, a magnetically suppressed tube is found extremely superior over the old tube with small aperture electrodes. The new tube has worked very satisfactorily for about six months since it was constructed.

In the following, the characteristics of new accelerating tube are described and compared with those of old one.

2. Structures of accelerating tubes

In Fig. 1 are shown the unit structures of the old and of the new accelerating

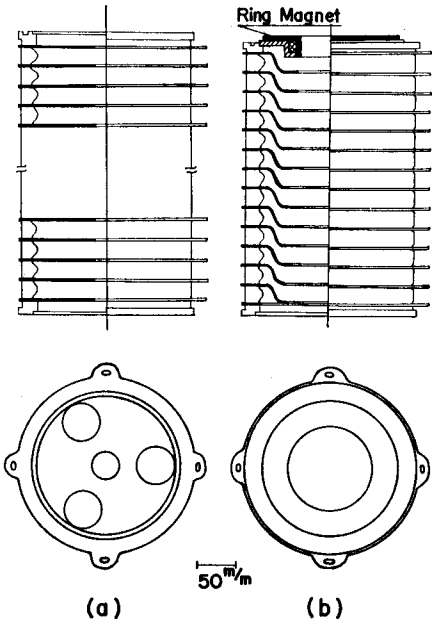

Fig. 1. Unit structure of the accelerating tube. (a) old tube, (b) new tube.

tubes.

The plane electrodes of the old tube are made of 1mm thick stainless steel (S-US 24) and cemented to a porcelain column with Araldite under high temperature. Each electrode has a central hole of 20mm in diameter and three pumping holes of 50 mm in diameter toward its outer part. These holes have been arranged so that they do not line up. Four such units form the old accelerating tube as shown in Fig. 2 (a).

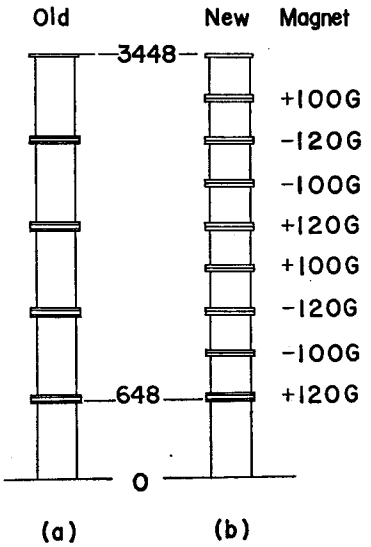

Fig. 2. Constructions of the accelerating tubes. (a) old tube, (b) new tube.

The electrodes of the new tube* are bucket type with central holes of linearly increasing diameters from 87 mm to 120 mm. Eight such units with respective permanent ring magnets** are piled up to form the new accelerating tube. Ring magnets are magnetized diametrically and suppress the electrons to pass up through the tube. The strengths and directions of magnetization of these magnets must be determined so that the deflection angle and the displacement of the ion beam after acceleration are diminished. The methods of calculation are given in Appendix 1. The arrangement of magnets in our tube is shown in Fig. 2 (b).

* The body of the new accelerating tube was produced by Mitsubishi Electric Corporation.

** The permanent ring magnets (NKS 1B) are 86 mm in inner diameter, 105 mm in outer diameter and 15 mm in thickness, and were produced by Sumitomo Special Metals Co. Ltd. The amount of outgas from one ring magnet was measured to be less than 0.03×10^{-5} Torr·l/sec, which is very small compared with the amout of outgas from the inner surface of the new accelerating tube, $(8 \sim 11) \times 10^{-5}$ Torr·l/sec.

3. Evacuation-characteristics of accelerating tubes

The conductance of the accelerating tube is evaluated from the equilibrium pressures at the top of the tube, $P(O)$, and at the lower end of the tube, $P(L)$, with the constant gas flow from the ion source mounted on the top of the tube. In general, there are some quantity of outgas from the inner surface of the tube and unexpected leakage from the connecting part of the ion source and the tube. In spite of this uncontrollable gas flow we can evaluate the conductance C of the tube from the following equation which is derived in Appendix 2 :

$$C\{P(O)-P(L)\} = \frac{Q_{out}}{Z}+Q_0+Q_1$$

where Q_{out} is the rate of outgas from the inner surface of the tube, Q_0 is that of the unexpected leakage of gas from the top of the tube and Q_1 is that of the controlled gas flow from the ion source. When Q_1 is plotted as a function of $P(O)$-$P(L)$, a linear relation is obtained. The gradient of this straight line immediately gives the value of the conductance C.

Table 1. Conductances of the accelerating tubes

	Experimental (l/s)	Theoretical	
		Independent holes (l/s)	Pipe approximation (l/s)
Old tube	5.4	5.7	6.3
New tube	19.2	5.3	20.2

In Table 1, there are given the experimental values of the conductance for the old and the new tubes in comparison with the theoretically calculated ones. The conductance of the new tube is about 4 times as large as that of the old tube. Theoretical calculation of "independent holes" means the approximation that holes in the electrodes and insulating columns are treated as independent conductances and being connected in series. In the "pipe approximation", the series of central apertures are regarded as a pipe of the same diameter as those of apertures for the old tube and a pipe with the minimum diameter of those of apertures for the new tube. It is clearly seen in Table 1 that the experimental value of the old tube is in better agreement with the theoretical value of "independent holes", while for the new tube, the pipe approximation" reproduces the experimental value very well. This difference might be caused by the different degree of contribution of the reflection of gas molecules from the wall of the fictitious pipe. For the small pipe, the reflection from the wall has too much contribution to the theoretical value, while

for the large pipe, this contribution is small compared with that passing through the pipe.

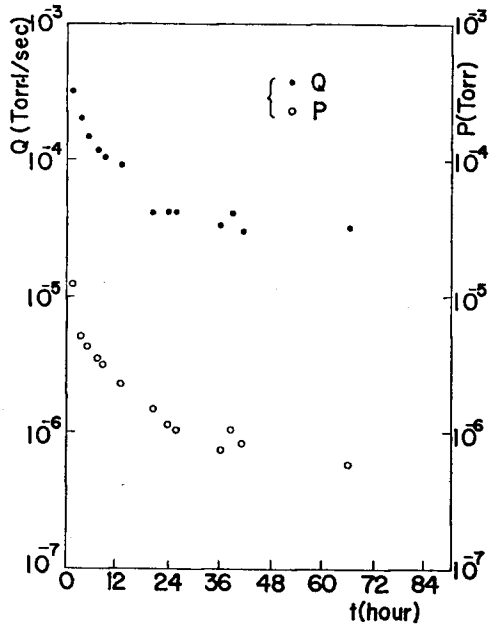

Fig. 3. Features of evacuation of the new tube. P : pressure at the lower end of the tube, Q : total leak-rate of the tube.

The features of evacuation immediately after the construction of new accelerating tube is shown in Fig. 3.

4. Electron loading

As a measure of the electron loading, we have measured the X-ray yields and the energy spectra of the X-rays at the various points of the accelerating tubes. The X-rays were detected by a $1\frac{3}{4}$-in. × 2-in. NaI scintillator surrounded by a lead shield with a thickness of 10cm with a collimating hole 1cm in diameter in the front lead block. This shield is sufficient to prevent the scattered X-rays from being detected, and only collimated X-rays through the front hole are detected. The assembly of the lead-shielded scintillator was moved up and down by an electric crane along a guide rail parallel to the axis of the accelerating tube. The arrangement of the measurement is shown in Fig. 4, in which the position of the scintillation detector is indicated.

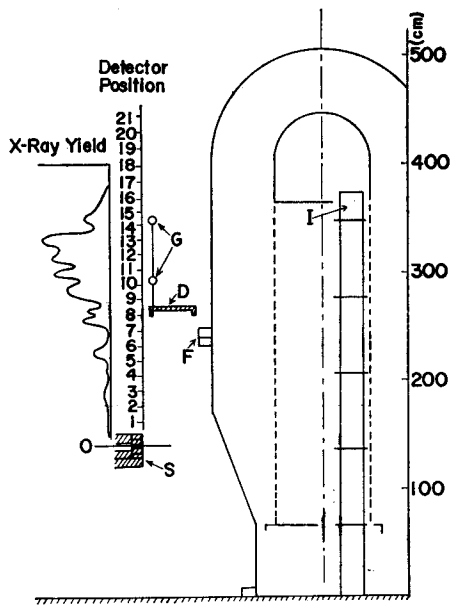

Fig. 4. Arrangement of the X-ray measurement. D : deck, G ; guardrail, S : scintillation detector assembly, I : ion source.

4-1 Old accelerating tube

The results of the measurement of the X-rays for the old accelerating tube are shown in Figs. 5, 6 and 7.

Fig. 5 (a) and (b) are the curves of X-ray yield as a function of the detector position for the acceleration of 20 μA* hydrogen ion beam by 1 and 3 MV, respectively. The output pulses from the detector were amplified and discriminated so that the X-rays of which energies were larger than 0.05 MeV and 0.5 MeV were counted in ratemeters and drawn on a two pen recorder. The position of the detector was continually changed by the electric crane. Fig. 5 (c) shows the curves for the acceleration of the 10 μA nitrogen ion beam by 3 MV. The curves in Fig. 5 (b) and (c) are different only in their scales. This means that the intensity of the backstreaming electrons for the acceleration of nitrogen ions is about twice that of hydrogen ions. We will later consider this point.

In any of the curves, one can see clearly the dips of X-ray yields corresponding to the attenuations by the frange of a high pressure tank, the deck for walking, and the guardrail. After correction of these absorptions, it may be concluded that the

* The ion beam current does not mean the accelerated total beam current but a part of it which is measured with the Faraday cup placed just below the steering electrodes at the end of the accelerating tube.

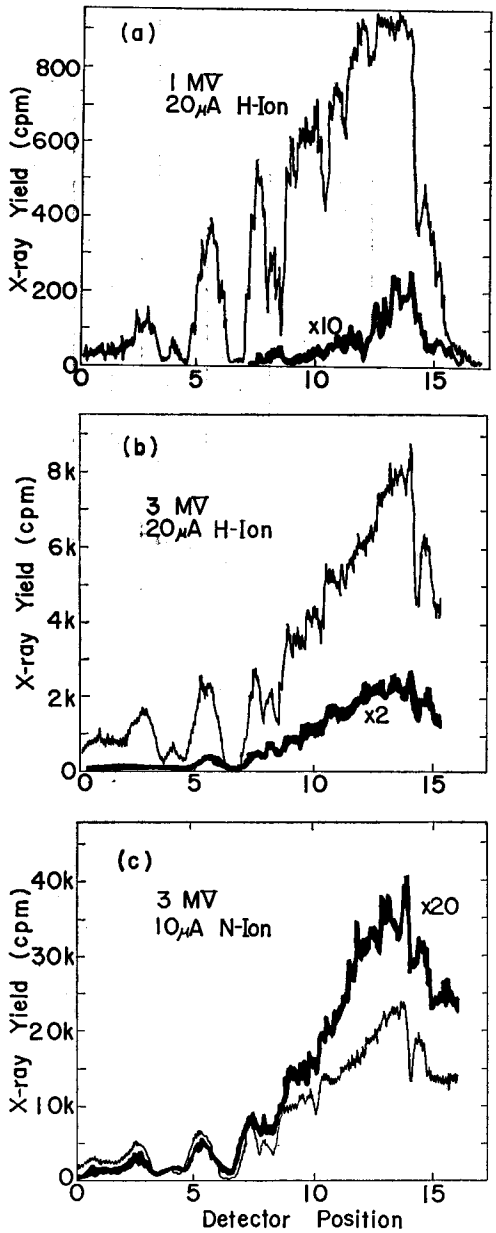

Fig. 5. X-ray yield as a function of the detector position for the old tube. ——: >0.5 MeV, ——: >0.05 MeV.

X-ray yield increases exponentially as the position goes up. This suggests that the secondary electrons produced at the lower part of the accelerating tube are accelerated upward, multiplying electrons by the collsions with electrode plates.

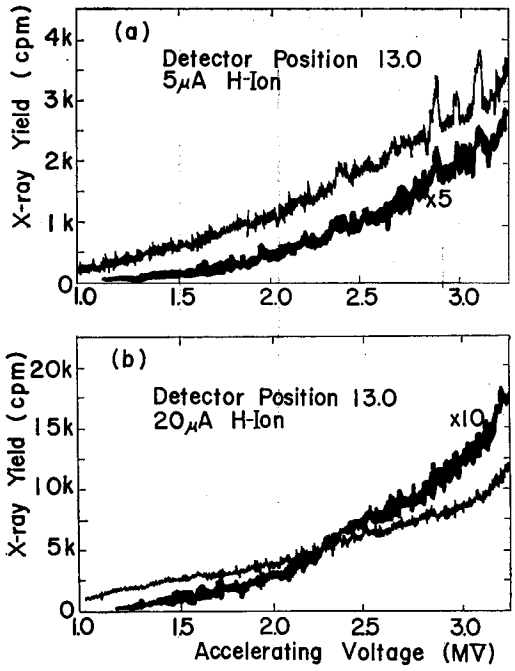

Fig. 6. X-ray yield for the old tube as a function of the accelerating voltage in the case of hydrogen ions. (a) 5 μA, (b) 20 μA.

Fig. 6 shows the change of X-ray yields with the accelerating voltage. The detector was set at the position of maximum X-ray yield near the ion source. Fig. 6 (a) and (b) are the curves for the accelerations of hydrogen ion beams of 5 μA and 20 μA, respectively.

In order to see the place of the production of backstreaming electrons, high voltage was applied to the steering electrodes placed directly under the accelerating tube whereby the ion beam would hit the defining slits below the steering electrode. The curve of X-ray yield vs position was not changed by this procedure. The place of the production of the backstreaming electrons, therefore, should be above the steering electrodes.

Measurements of the energy spectra of X-rays were made at the position of 0, 4, 9 and 13. The output pulses from the scintillation detector were analysed on a pulse-height-analyzer. The pulse height distributions are shown in Fig. 7. In order to obtain the energy spectra of X-rays from these pulse height distributions, it is necessary to correct the absorption in the tank wall and to unfold the distribution by using the response function of the scintillator. In the present range of energies, however, the pulse height distribution itself is a good approximation of the energy

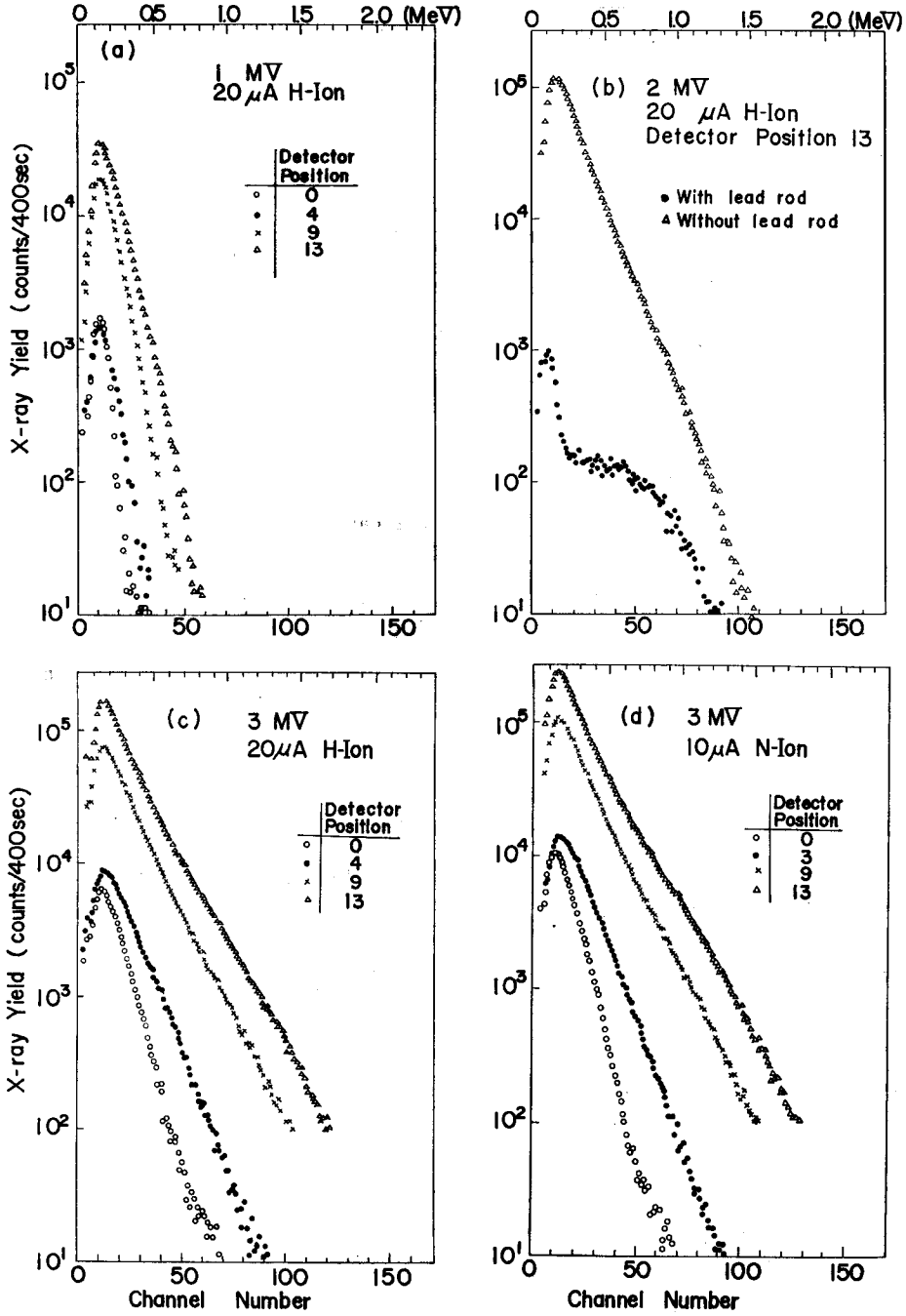

Fig. 7. Energy spectra of X-rays of the old tube. (a) 1 MV (Hydrogen ion), (b) 2 MV (Hydrogen ion), (c) 3 MV (Hydrogen ion), (d) 3 MV (Nitrogen ion).

distribution. Further, as shown in Fig. 7 (b), the background X-rays measured with a lead rod in the front hole of lead shield was very low compared with the collimated X-rays. Procedure of subtraction of the background spectrum may be omitted as long as one considers the channel number at which the count is from one hundredth to one thousandth of the count at the peak channel number. Therefore, in the following we take the raw pulse height distribution for the energy distribution of X-rays.

In Fig. 7 (a), (b) and (c) are shown the X-ray spectra at the representative positions for the accelerations of 20 μA hydrogen ion beams by 1, 2 and 3 MV, respectively. The apparent peaks at about 0.15 MeV in these spectra are due to the strong absorption of low energy X-rays in the tank wall. The absorption coefficient of X-rays in iron is known to increase rapidly when the energy of X-rays decreases below 0.15 MeV.

From these figures, it is clear that the energy of X-rays increases with the raising of the accelerating voltage. These facts can be explained by backstreaming electrons originated at the lower part of the accelerating tube.

Fig. 7 (d) shows the spectrum for the acceleration of 10 μA nitrogen ion beams by 3 MV. The shapes of these spectra are the same as the corresponding ones for 20 μA hydrogen ion beams (Fig. 7 (c)) except that the absolute magnitudes of the intensities of the former are about 1.5 times as large as those of the latter. This means that the rates of increase of X-ray yield due to the multiplication of secondary electrons are the same for hydrogen ions and for nitrogen ions, and that the effective number of secondary electrons produced by the nitrogen ions at the lower part of the tube is about 1.5 times as large as that by the hydrogen ions.

This does not necessarily mean that the secondary electron yield of nitrogen ion is 1.5 times as large as that of hydrogen ion. Possibly, the convergence of the nitrogen ion beam may be poorer than that of the hydrogen ion beam, and more ions of nitrogen than those of hydrogen may bombard the place for electron production. It is to be noted, as has been mentioned in the footnote on p. 62, that the ion beam current used above is the current of the Faraday cup, and the accelerated ion current in the tube is larger than this current.

To determine whether the middle electrodes become the place for production of secondary electrons, the X-ray yields and energy spectra were compared for divergent beam and convergent beam. There was no difference between these two results. Therefore, it is certain that the place of production of secondary electrons is in the lower part of the accelerating tube.

4-2 New accelerating tube

The curves of X-ray yields vs position for the new accelerating tube are shown

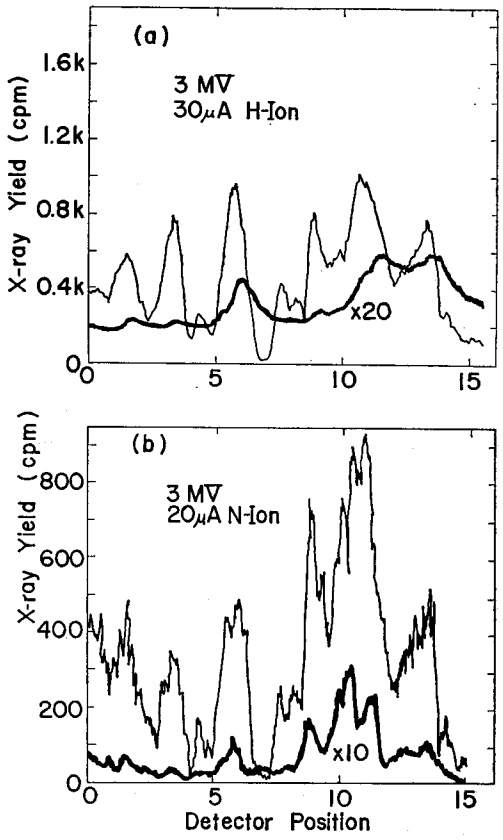

Fig. 8. X-ray yield for the new tube as a function of the detector position. (a) 3 MV (Hydrogen), (b) 3 MV (Nitrogen ion).

in Fig. 8, (a) representing the 30 μA hydrogen ion beam and (b) the 20 μA nitrogen ion beam, respectively. There are marked differences between these curves and the corresponding ones of the old accelerating tube as shown in Fig. 5 (b) and (c).

Firstly, the rate of increase of the X-ray yield at a higher position is very small in the new accelerating tube compared with that in the old tube. In particular, for the acceleration of hydrogen ions, X-ray yields at any position of the new tube are almost constant on the average. Secondly, the X-ray yields in the new tube are about one hundredth of those in the old tube. It is evident that the ring magnets work very well to suppress the backstreaming electrons.

In order to see more fully the relation between X-ray yields and the position, the assembly of the scintillation detector was changed to the opposite side of the tank. In this arrangement, the distance between the scintillator and the accelerating tube becomes about 3/4 of the previous arrangement.

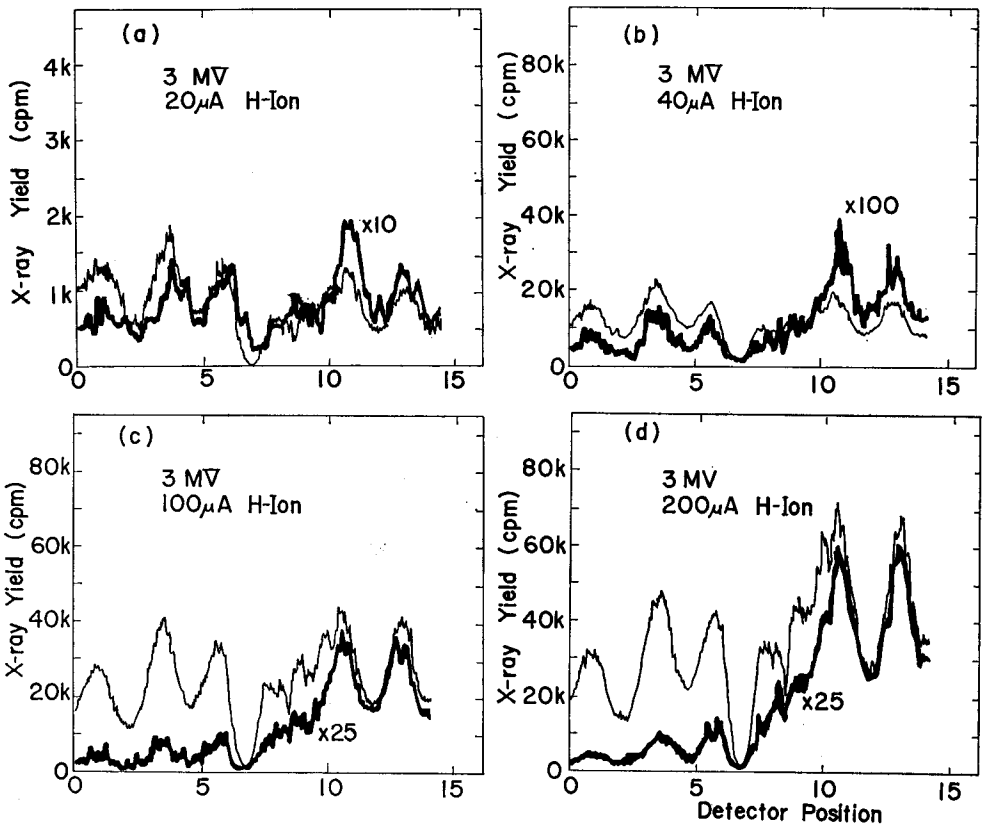

Fig. 9. X-ray yield for the new tube as a function of the detector position for the acceleration of hydrogen ion beam by 3 MV. (a) 20 μA, (b) 40 μA, (c) 100 μA, (d) 200 μA.

The curves of X-ray yield vs position obtained in the new arrangement are shown in Figs. 9 and 10. Figs. 9 (a), (b), (c) and (d) are the curves for the 3 MV-acceleration of hydrogen ion beam of 20, 40, 100 and 200 μA, respectively. Fig. 10 (a) and (b) show the curves for the 3 MV-acceleration of nitrogen ion beam of 40 and 100 μA, respectively. They show that the rates of increase of X-ray yields at a higher position are larger for a larger ion beam current. The intensity of X-rays of Fig. 10 (a) is between those of Fig. 9 (b) and (c) ; and a similar relation is true for the rates of increase of X-ray yield for a higher position.

Further, the X-ray yields shown in Fig. 10 (b) are larger than those in Fig. 9

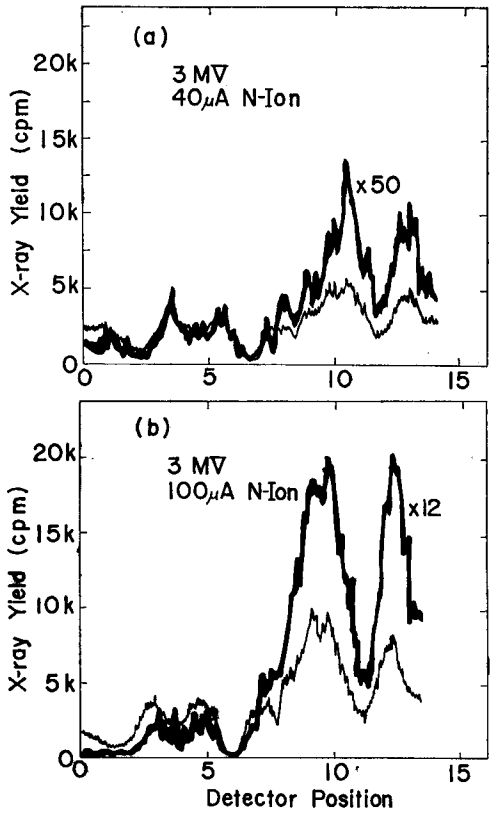

Fig. 10. X-ray yield for the new tube as a function of the detector position for the acceleration of nitrogen ion beam by 3 MV. (a) 40 μA, (b) 100 μA.

(d) and, correspondingly, the rate of increase of the X-ray yield of the former is larger than that of the latter. From these facts, the pattern of the increase of X-rays seems to be determined by the intesity of X-rays and independent of the kind of accelerated ions.

The changes of the X-ray yield with the ion beam current were measured at a fixed position and with a fixed accelerating voltage. They are shown in Fig. 11 (a) and (b). The X-ray yield increases almost linearly with an increase of the beam curent. The small deviations from the linear relation may be attributed to the condition of the beam convergence.

Fig. 12 (a) and (b) show the changes of the X-ray yield with accelerating voltage for a fixed intensity of the accelerated beam. The intensities of X-rays are different, but features of the changes are the same for both curves.

The energy spectra of X-rays of the new tube showed marked difference from

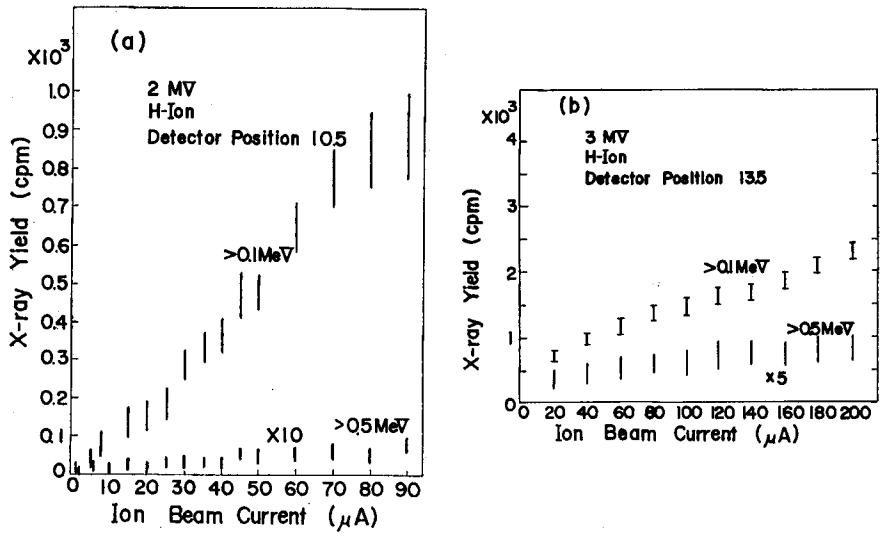

Fig. 11. X-ray yield for the new tube as a function of the hydrogen ion beam current. (a) 2 MV, (b) 3 MV.

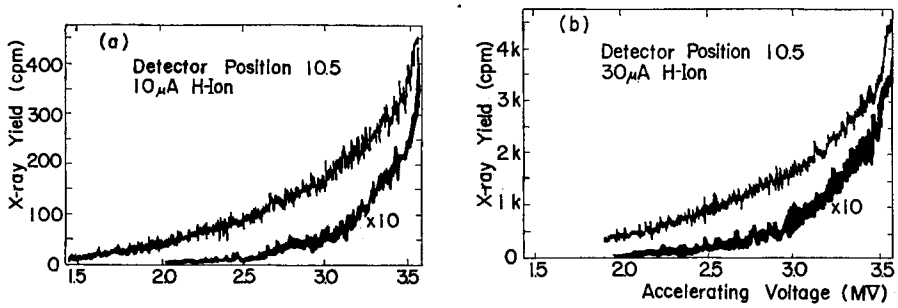

Fig. 12. X-ray yield for the new tube as a function of the accelerating voltage in the case of hydrogen ions. (a) 10 μA, (b) 30 μA.

those of the old tube. In Fig. 13 (a), (b) and (c) are shown the energy spectra of X-rays measured at the positions of 0, 3.2, 10.3 and 13.0, respectively. For comparison, the spectra at position 0 of the old tube with similar conditions of operation are drawn in Fig. 13 (b) and (c). The energy spectra of X-rays at any position of the new tube are almost the same as those of the old tube at the lowest position. This means that the ring magnets are very effective for the suppression of electrons so that the backstreaming electrons are completely confined in each unit of the accelerating tube.

The typical distribution of X-ray doses in the accelerator-room and in the experimental room are shown in Fig. 14.

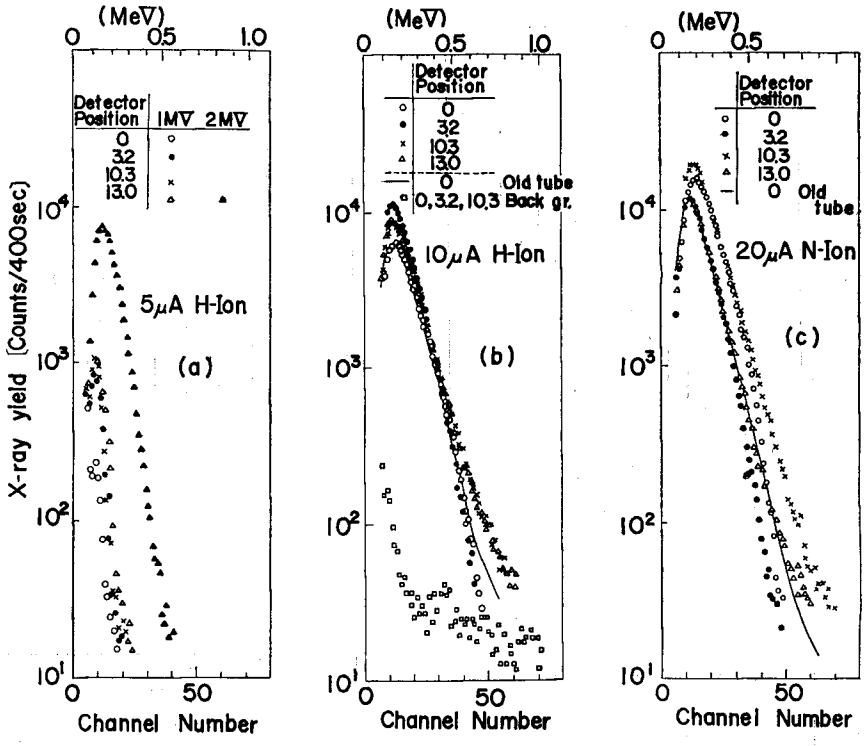

Fig. 13. Energy spectra of X-rays of the new tube. (a) 1 MV and 2 MV (Hydrogen ion), (b) 3 MV (Hydrogen ion), (c) 2 MV (Nitrogen ion).

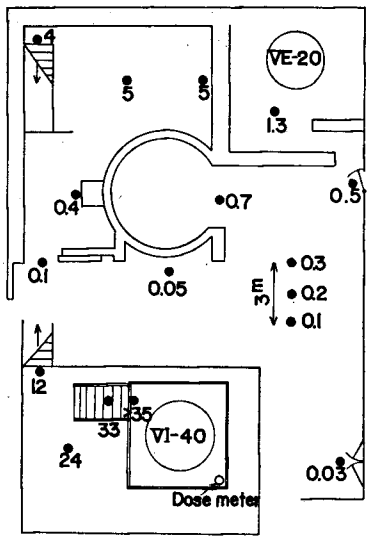

Fig. 14. Typical distribution of X-ray doses (in unit of mR/h) around the accelerator.

5. Characteristics of beam convergence

In order to obtain a well focused beam, it is necessary to adjust the extraction voltage and the lens voltage. The optimum values of these voltages strongly depend upon the condition of the discharge in the ion source. The following are the average characteristics.

The ion source is a cold cathode PIG type and ions are extracted axially through the aperture (1mm in diameter) in the cathode. Fig. 15 (a), (b) and (c) show the changes of the hydrogen ion beam current with the extraction voltage and the lens voltage for 1, 2 and 3 MV-accelerations, respectively. The defining slits just above

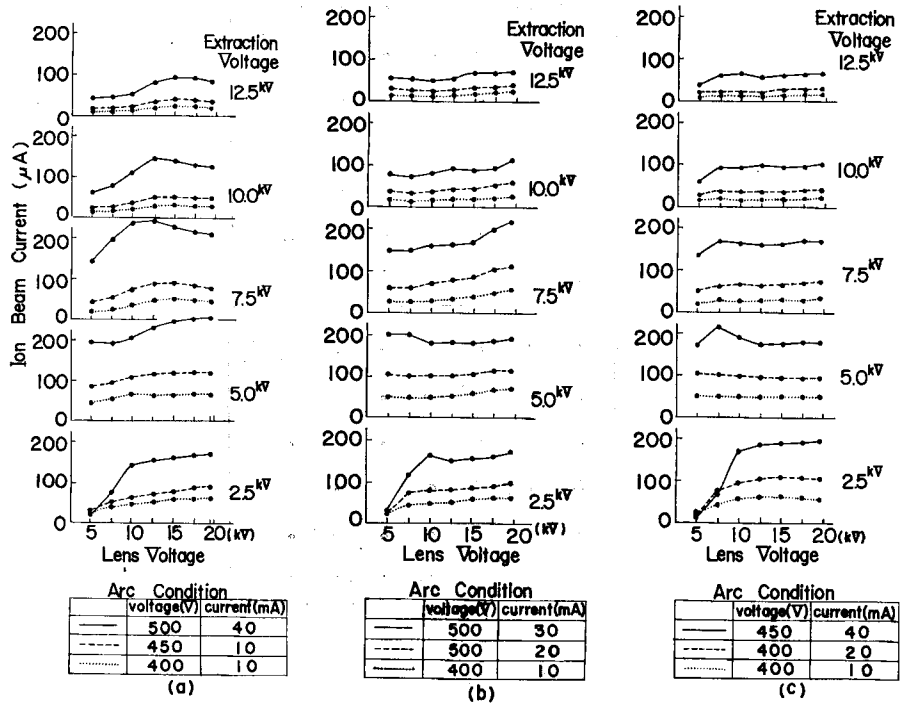

Fig. 15. Change of hydrogen ion beam current with extraction voltage, lens voltage and arc voltage of the ion source. (a) 1 MV, (b) 2 MV, (c) 3 MV.

the Farady cup were widely opened as large as 40 mm × 40 mm. It can be seen from these figures that, for any accelerating voltage, the lens voltage should be larger (above 10KV) and the extraction voltage should not be too large in order to obtain a large ion beam current.

The sizes of beam spots were measured on a quartz plate covered with nickel-net of mesh size 1.25 mm which was inserted just above the Faraday cup. In these

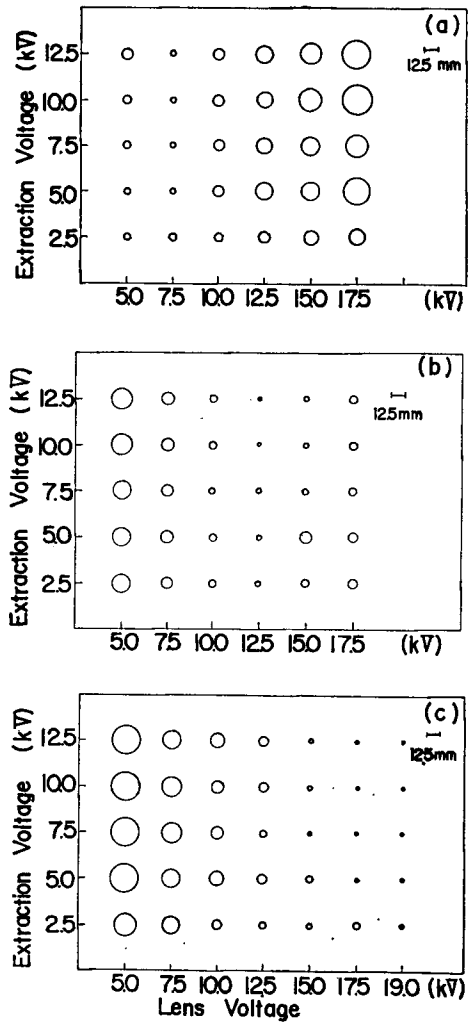

Fig. 16. Sizes of beam-spots of hydrogen ion for some combinations of extraction voltage and lens voltage. (a) 1 MV, (b) 2 MV, (c) 3 MV.

measurements, the ion beam currents were limited to 1 μA so that the fluorescent spot could be easily observed. For the accelerating voltages of 1, 2 and 3 MV the sizes of beam spots of hydrogen ion beams are depicted in Fig. 16 for some combinations of the extraction voltage and the lens voltage. It is clearly seen in these figures that a well focused beam is obtained if the lens voltage was made large when the accelerating voltage was large. The extraction voltage has little effect on the convergence of the ion beam.

With the assumption that the beam converegence is independent of the ion

Table 2. Recommended values of the extraction- and lens-voltages for hydrogen ion beam.

Accelerating voltage (MV)		1	2	3
Extraction voltage	(kV)	7.5	7.5	7.5
Lens voltage	(kV)	7.5	12.5	17.5

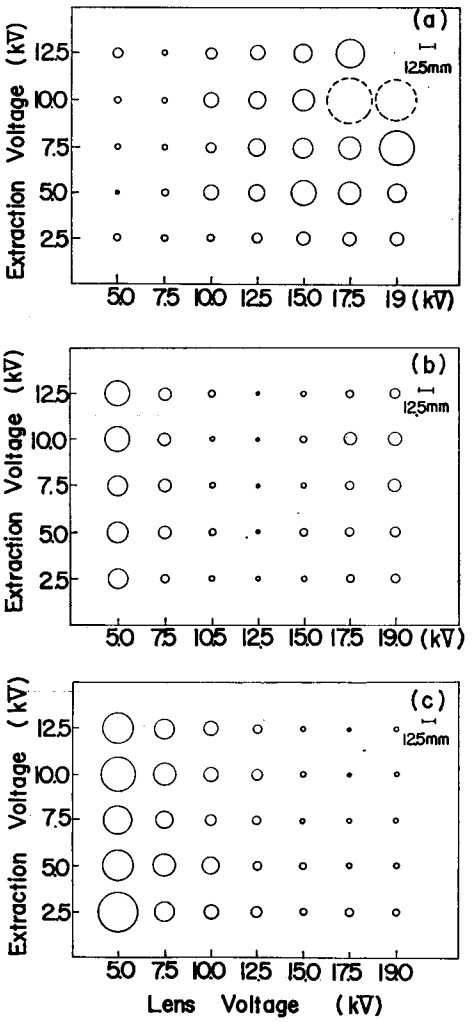

Fig. 17. Sizes of beam-spots of nitrogen ion for some combinations of extraction voltage and lens voltage. (a) 1 MV, (b) 2 MV, (c) 3 MV.

beam current, one gets the following conclusion by combining the above two results of beam intensity and of convergence. For a well focused intense beam, it is recommended to give an extraction voltage of less than 7.5 kV and a lens voltage of smaller or larger values corresponding to the accelerating voltage. The optimum combinations for hydrogen ion acceleration are given in Table 2.

For nitrogen ion acceleration the sizes of beam spots are depicted in Fig. 17 (a), (b) and (c). The features of changes are similar to those of the hydrogen ion beam, but more sensitive to the lens voltage. For nitrogen ions, therefore, the setting of the lens voltage must be more careful than that for hydrogen ions.

6. Characteristics of operation

Even with a constant accelerating voltage, the divider-current decreased when the ion beam current increased. This fact is due to the backstreaming electrons flowed into the divider resistance through the electrodes. In order to keep the accelerating voltage constant, therefore, this electron-load current must be supplemented by increasing a spray current onto the charge-carrying belt. The relations between these currents are fundamental ones for the operation of the accelerator, and are given in the following for standard cases.

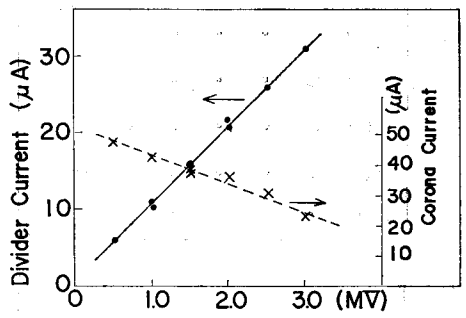

Fig. 18. Relation between divider-current and the accelerating voltage for no ion beam.

Fig. 18 shows the relation between the divider-current and the accelerating voltage for no ion beam. The spray current was kept constant and the accelerating voltage was set up by changing the distance between the corona point and the shielding case at a high voltage terminal. The divider-current increased linearly with the increase of the terminal voltage, and the following relation held very well.

$$\text{Spray current} = \text{Divider-current} + \text{Corona current}$$

This means that the leakage currents of the insulating column and the corona current of the pressure tank may be disregarded in the present considerations.

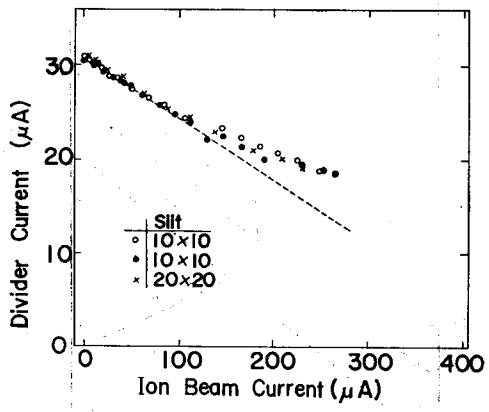

Fig. 19. Relation between divider-current and hydrogen ion beam current at the accelerating voltage of 3 MV.

Fig. 19 shows the changes of the divider-current with the increase of the hydrogen ion beam current at the accelerating voltage of 3 MV. As shown in Appendix 3, the divider-current should decrease linearly with an increase of ion beam current. Meanwhile, the rate of decrease of the divider-current becomes slower at larger ion beam currents. For an explanation of the deviation from the linear relation, it is necessary to assume a different mechansim of electron multiplication for each different ion beam current. As will soon be shown the value of the current measured on the Faraday cup was about 1.3 times as large as the true value of the ion current. After correction of this factor, the dotted line shown in the figure may be considered as a good approximation of the relation within the experimental errors.

Fig. 20 and 21 show the relations of currents at the accelerating voltage of 2 MV for hydrogen ions and nitrogen ions, respectively. In Fig. 20, the dotted line shows the (Spray current) − (Divider current) − (Corona current), which should be equal to the ion beam current. The difference between the really accelerated ion beam current and that of Faraday cup, a factor of about 1.3, may be attributed to the escape of secondary electrons from the Faraday cup.

Table 3. Maximum ion beam currents

		Hydrogen ion		Nitrogen ion	
Accelerating voltage	(MV)	2	3	2	3
Maximum current	(μA)	400	200	180	150
Permitted current for stable operation	(μA)	350	200	180	120

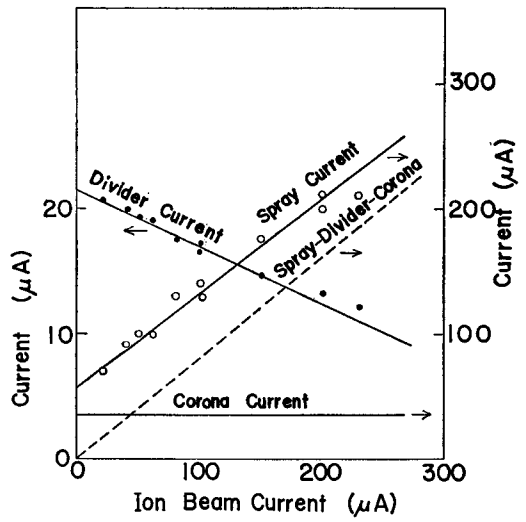

Fig. 20. Relation of currents (beam, spray, divider and corona) for hydrogen ion at the accelerating voltage of 2 MV.

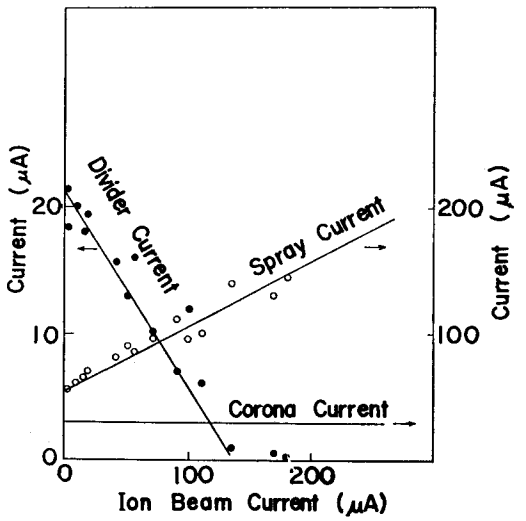

Fig. 21. Relation of currents (beam, spray, divider and corona) for nitrogen ion at the accelerating voltage of 2 MV.

The maximum ion beam currents obtained so far by the new accelerating tube are given in Table 3.

Only two days after it was constructed, the new accelerating tube permitted the terminal voltage to be raised up to 3.8 MV without ion beam and up to 3.6 MV with 40 μA hydrogen ion beam. In contrast to this, for the old tube, the maximum

accelerating voltage of 3.2 MV with 20 μA hydrogen ion beam was realized after a fairly long time of conditioning. The effect of conditioning for the new tube holds so long that the terminal voltage is allowed to rise immediately up to 80~90% of the voltage which had been raised before one day.

The relations between the X-ray dose and the beam current are shown in Fig.

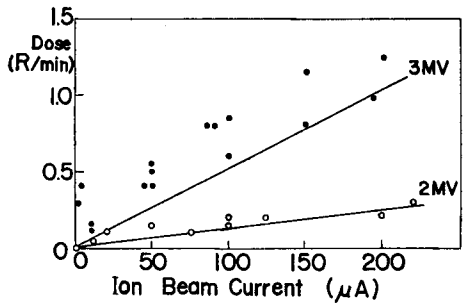

Fig. 22. Relation between X-ray dose and hydrogen ion beam current.

22. The X-ray dose was measured with the dose-monitor (ionization chamber) placed near the accelerator. The scattering of the experimental values might be due to the degree of covergence of the beam, and the straight lines give the lower limits for the X-ray dose.

7. Ion-characteristics of the accelerated beam

The atomic ratio and the charge distribution of the accelerated ion beam depend upon the pressure in the ion source and on the condition of discharge in it. Especially, the charge distributions of ions change markedly with fine changes of the shape of the cathode of the ion source. However, as long as the cathode is as good as new, the following characteristics are the typical.

In Fig. 23 are shown the ion-contents of the accelerated beams analyzed with a 90° bending magnet. For the acceleration of argon ions (Fig. 23 (d)) it is interesting to note that there is a considerable amount of Al^+ ions other than argon ions. These Al^+ ions were produced by the sputtering of the aluminum cathode. By utilizing another metal for the cathode material one may obtain the ions of that metal. On the other hand, large cathode-sputtering is undesirable as regards the lifetime of the ion source. For example, the ion source with an aluminum cathode lasts for about one month with hydrogen gas but for only a few days with argon gas. For the acceleration of heavy ions, therefore, it is strongly suggested to seek cathode material with a less sputtering ratio or to construct a newly designed ion source to overcome the above defect.

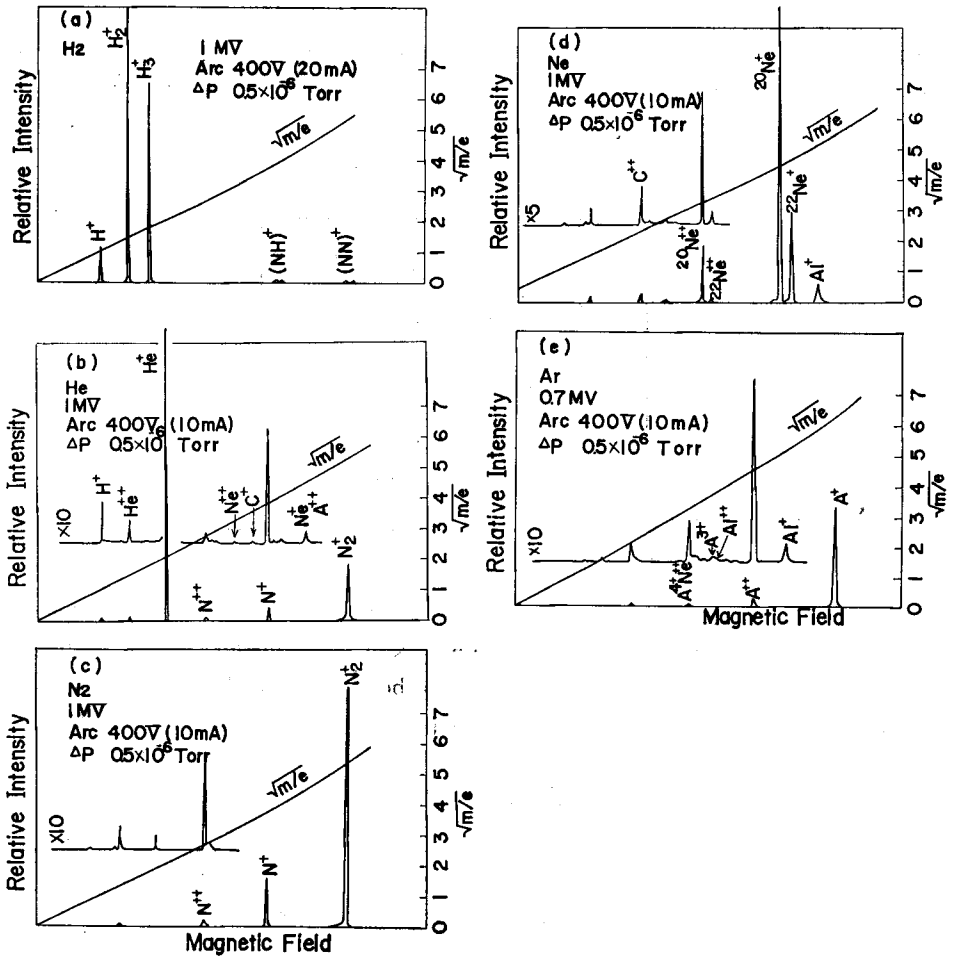

Fig. 23. Ion-contents of the accelerated beams analyzed with a 90° magnet. (a) Hydrogen, (b) Helium, (c) Nitrogen, (d) Neon, (e) Argon.

8. Conclusions

The newly constructed accelerating tube with ring magnets has a conductance about 4 times larger than that of the old tube and good quality for the suppression of the backstreaming electrons. The amount of electron loading was reduced by a factor of 100 and the beam current was increased by a factor of about five in comparison with those of the old tube. These improvements facilitate the operation of the accelerator and considerably decreased the X-ray dose in the neighbourhood of the accelerator. A long keeping of the conditioning effect saves the time of operation very much.

The structure of the new accelerating tube is simpler than that of the inclined tube. The magnetically suppressed accelerating tube may be the most favorable type of the accelerating tube. A remaining problem on the improvement of the static accelerator is above all the improvement of the ion source, especially for heavy ion accelerations.

Acknowledgements

We wish to thank Professor A. Isoya of Kyushu University for valuable suggestions and advice on the technique of magnetic suppression. The help of the following members during the construction and measurement is gratefully acknowledged : Drs M. Mannami, T. Nakamura, Messrs H. Fujita, K. Shima, K. Sone, H. Maruhashi, M. Takasaki, T. Oshiyama, H. Hirayama, S. Nishino, N. Sakamoto, M. Teramoto, H. Kudo, N. Sawano, J. Ozaki, Y. Yamanaka, Y. Terashima, and T. Inagaki. We also wish to thank Mr. Y. Inoue, Mitsubishi Electric Corporation, for many valuable discussions.

Appendix 1. Magnets for the suppression of electron loading

For the suppression of the backstreaming electrons, magnets with a transverse field to the axis of the accelerating tube may be used. The arrangement of the magnets must be such that the net effect of the magnetic fields to the accelerated ion beam cancels out. After acceleration

(1) the deflection angle of the ion beam from the axis of accelerating tube is zero, and

(2) the horizontal displacement of the ion beam is zero

In the following, the conditions of the magnets for these two requirements are derived.

When the ion with charge e, mass m and velocity v pass through the magnetic field B of length ΔL, the change of the direction of motion, θ, is given by

$$\sin\theta = \frac{eB\Delta L}{mv}$$

and the acquired transverse velocity Δv_T is given by

$$\Delta v_T = v\sin\theta = \frac{eB\Delta L}{m}.$$

The transverse velocity after passing through a magnet is

$$v_T = \frac{e}{m}\int_{-\infty}^{\infty} BdL = \frac{e}{m}A, \qquad (1)$$

where A is the integrated magnetic field. It is to be noted that v_T is independent

of the ion energy.

If N magnets are arranged so that directions of their magnetic field are parallel with one another along the accelerating tube, the ion beam accelerated by a voltage of V has a deflection angle Θ_N at the outlet of the accelerating tube.

$$\Theta_N = \sum_{i=1}^{N} v_{Ti} \Big/ \sqrt{\frac{2eV}{m}}$$

$$= \sqrt{\frac{1}{2}\frac{e}{m}\frac{1}{V}} \sum_{i=1}^{N} A_i. \tag{2}$$

The requirement of zero deflection angle is fulfilled if

$$\sum_{i=1}^{N} A_i = 0. \tag{3}$$

Assume the ion velocity at the entry of tube as zero. If N magnets are set at the distance $l_1, l_2, \cdots, l_N$ $(= l)$ from the tube's entrance the times of, passage of these magnets $t_1, t_2, \cdots t_N$ are given by

$$t_i = \sqrt{2\frac{m}{e}\frac{l}{V}}\, l_i \qquad (i = 1, 2, \cdots N). \tag{4}$$

Transverse velocity u_i after passing through the i-th magnet is

$$u_i = \sum_{k=1}^{i} v_{Tk} = \sum_{k=1}^{i} \frac{e}{m} A_k. \tag{5}$$

Combining Eqs. (4) and (5) one obtains the displacement of beam a_N after passing through the N-th magnet.

$$a_N = \sum_{i=1}^{N-1} u_i (t_{i+1} - t_i)$$

$$= \frac{e}{m} \sum_{i=1}^{N-1} \sum_{k=1}^{i} A_k (t_{i+1} - t_i)$$

$$= \frac{e}{m} \left(t_N \sum_{i=1}^{N-1} A_i - \sum_{i=1}^{N-1} A_i t_i \right)$$

$$= \sqrt{2\frac{e}{m}\frac{l}{V}} \left(\sqrt{l} \sum_{i=1}^{N-1} A_i - \sum_{i=1}^{N-1} \sqrt{l_i}\, A_i \right) \tag{6}$$

The requirement of zero displacement is satisfied if

$$\sqrt{l} \sum_{i=1}^{N-1} \sqrt{A_i} - \sum_{i=1}^{N-1} \sqrt{l_i}\, A_i = 0. \tag{7}$$

By using Eq. (3), Eq. (7) becomes

$$\sum_{i=1}^{N}\sqrt{l_i}\,A_i = 0. \tag{8}$$

When the magnets are set with an equal interval, that is, $l_i = \frac{i}{N}l$, Eq. (8) becomes

$$\sum_{i=1}^{N}\sqrt{i}\,A_i = 0. \tag{9}$$

When the field directions of successive eight magnets are altered in a sequence as $+--++--+$, Eqs. (3) and (9) are satisfied if

$$\begin{aligned} &|A_1| = |A_3| = |A_5| = |A_7| \\ &|A_2| = |A_4| = |A_6| = |A_8| \\ &|A_2| = 1.185\,|A_1|. \end{aligned} \tag{10}$$

We have used the diametrically magnetized ring magnets of 1.5 cm in thickness and of 100 and 120 Gauss in the strenght of field at the centers. Integrated fields are approximately given by

$$\begin{aligned} |A_1| &= 100\times 1.5\ Gauss\cdot cm \\ |A_2| &= 120\times 1.5\ Gauss\cdot cm \end{aligned} \tag{11}$$

The difference of the values of Eqs. (11) from those of Eqs. (10) causes non-zero displacement, but it is very small. For example, for 0.6 MeV proton a_N = 0.04 mm, which is negligible.

Appendix 2. Measurement of the conductance of the accelerating tube with outgas and leakage

Let $P(x)$ be the pressure in the tube at the distance x from the top of the tube. The conductance of the small part of tube $(x,\ x+dx)$ is formally represented as $C\frac{L}{dx}$, where C is the conductance of the whole tube of length L. If there are gas leakage from the top of the tube and outgas from the inner surface of the tube, the relation between the pressures and the quantity of flowing gas through the ion source are, in equilibrium,

$$\{P(x)-P(x+dx)\}\frac{CL}{dx} = qx+Q_0+Q_1,$$

where q is the outgas per unit length per unit time, Q_0 is the gas leakage per unit time and Q_1 is the controllable gas flow. By integration, one obtains

$$C\,[P(O)-P(L)] = \frac{Q_{out}}{2}+Q_0+Q_1$$

where

$$Q_{out} = qL = \text{total outgas.}$$

From the experimental values of $P(O)$ and $P(L)$ for various Q_1, one can calculate C and $\frac{Q_{out}}{2} + Q_0$.

Appendix 3. Change of divider-current with varying ion current

The divider-current was measured with the current meter at the end of the divider resistance. It then apparently decreases when the backstreaming electrons collide with the accelerating electrodes and enter the divider resistance.

If the backstreaming electron current $i(x)\,dx$ enter a distance $(x, x+dx)$ from the top of the accelerating tube, the apparent decrease of divider-current is

$$-dI = \frac{x}{L}\, i(x)\, dx$$

where L is the length of the accelerating tube. Integration over the whole tube gives

$$-I_{dec} = -\int dI = \frac{1}{L}\int_0^L x\, i(x)\, dx$$

As the feature of electron multiplication in the accelerating tube is independent of the accelerated ion beam current,

$$i(x) = I_{ion}\, f(x)$$

where $f(x)$ is the pattern function of electron multiplication. Combining above two expressions, one obtains

$$-I_{dec} \propto I_{ion},$$

that is, the divider-current decreases linearly with an increasing ion current.

References

1) Electrostatic Generator Group, Department of Physics : Mem. Fac. Sci., Kyushu Univ., ser. B Phys. **4**, special issue (1970)
2) F. A. Howe : IEEE Transactions on Nuclear Science **14**, 122 (1967), ibid, **16**, 98 (1969)
3) S. Takayanagi, N. Terasawa, M. Mori and N. Kawai : Genshikaku Kenkyu (circular in Japanese), **9**, 395 (1964)
4) E. Teranishi and M. Kageyama : Genshikaku Kenkyu (circular in Japanese), **10**, 635 (1966)